Journal of Alloys and Compounds 523 (2012) 49–60

Contents lists available at SciVerse ScienceDirect

Journal of Alloys and Compounds

journal homepage: www.elsevier.com/locate/jallcom

Review

Influence of pH value, chloride ion concentration and immersion time on corrosion rate of friction stir welded AZ61A magnesium alloy weldments

A. Dhanapal[a,*], S. Rajendra Boopathy[b], V. Balasubramanian[c]

[a] Department of Mechanical Engineering, Sri Ramanujar Engineering College, Vandalur, Chennai 600048, Tamil Nadu, India
[b] Department of Mechanical Engineering, Anna University, Chennai 600025, India
[c] Centre for Materials Joining Research (CEMAJOR), Department of Manufacturing Engineering, Annamalai University, Annamalainagar 608002, India

ARTICLE INFO

Article history:
Received 27 July 2011
Received in revised form 6 January 2012
Accepted 15 January 2012
Available online 8 February 2012

Keywords:
Magnesium alloy
Friction stir welding
Immersion test
Weight loss
Corrosion rate

ABSTRACT

Magnesium alloys have gained considerable interest as a structural material for automotive and aerospace applications due to its low-density, high specific strength and good castability. As a consequence, this light alloys have a promising future. The limitation of low corrosion resistance restricts their practical applications. The corrosion behavior of friction stir welded AZ61A magnesium alloy welds was investigated by Immersion technique. Extruded Mg alloy plates of 6 mm thick of AZ61A grade were butt welded using friction stir welding (FSW) process. The present paper reveals the effect of pH, chloride ion concentration and immersion time on corrosion rate of friction stir welded AZ61A magnesium alloy welds in NaCl solution. The corrosion rate was evaluated from weight loss measurements. Furthermore, an attempt was made to develop an empirical relationship to predict the effect of pH value, chloride ion concentration and immersion time on corrosion rate of AZ61A magnesium alloy welds. The corrosion morphology observation was carried out by optical microscopy and the corrosion products were analyzed by SEM and XRD analysis.

Contents

* Corresponding author. Tel.: +91 44 22751393; mobile: +91 9444859455; fax: +91 44 22751370.
E-mail address: sridhanapal2010@gmail.com (A. Dhanapal).

0925-8388/$ – see front matter © 2012 Elsevier B.V. All rights reserved.
doi:10.1016/j.jallcom.2012.01.070

1. Introduction

Magnesium alloys, with a relatively high specific strength and excellent technological properties, have a high potential for use as a lightweight structural materials in automotive and aerospace applications [1]. However, application of these alloys requires welding and joining procedures to be developed. Unfortunately, the conventional fusion welding of Mg alloys often produces porosity in the weld joint, which deteriorates its mechanical properties, extremely the susceptibility to corrosion [2].

Hence, the applications of Mg alloys in structural members were still limited. However, a recent innovation of friction stir welding (FSW) process eliminated the above said problems. FSW is a solid state, autogenous process and hence there is no melting and solidification. Though the mechanical properties and microstructural characteristics of FSW joints of Mg alloys are the topic of many researchers, the corrosion properties of these joints have not yet been fully explored. Moreover, it significantly improves the weld properties and, hence extensively applied in joining magnesium alloys [3].

Immersion testing is the main technique for corrosion studies which was employed in this research in an effort to expose the AZ61 Mg alloy to an environment similar to that experienced by automotive engine blocks [4]. It is well-known that Mg alloys are susceptible to corrosion such as pitting and stress cracking corrosion (SCC). Major studies shows that the SCC susceptibility of Mg alloys is increased in solutions containing chloride [1,5]. The welding processes inevitably cause changes in the original microstructure of the alloy due to welding thermal cycles. These microstructural changes can affect the localized corrosion behavior of the alloy [6].

The pH of test solution has a considerable effect on the corrosion rate of Mg. However, it is difficult to keep it consistent especially in a neutral solution because the corrosion product of Mg, Mg hydroxide is readily dissolved into the solution which results in substantial pH increase [7]. The corrosion behavior of an AZ91 alloy in dilute chloride solutions was studied recently in which a corrosion map as in term of the electrode potential and Cl^- was obtained using electrochemical measurement. It was found that there is corrosion and passivation zones in diluted NaCl solutions and open circuit potential were located in the passivation zone when the Cl^- is less than 0.2 M and the corrosion zone as the Cl^- is higher than 0.2 M [8]. The typical microstructure of AZ91 has a primary α-phase and a divorced eutectic which consists of the β-phase ($Mg_{17}Al_{12}$) and the eutectic β phase distributed along a phase grain boundaries [9]. The relatively fine β phase network and the Al enrichment produced on the corroded surface of the AZ91 may be the key factors which limit the progressives of the corrosion attacks as comparing with AZ31 alloy [10,11]. Corrosion attacks of Mg, AZ31, AZ80 and AZ91D materials under the salt fog test increased with increasing temperature and Cl^- concentration [12]. Individual pitting characteristics, including pit surface area and pit volume, were greater for the salt spray surfaces [13].

It is well-known that the corrosion behavior of magnesium alloy greatly relates to the microstructure. For example, $Mg_{17}Al_{12}$ has a dual effect on the corrosion resistance of AZ91 Mg alloy, behaving as cathode to accelerate corrosion (or) a barrier to prevent corrosion [14,15]. Usually, the second phase in traditional Mg alloys consists of binary alloy such as $Mg_{17}Al_{12}$ and AlMn. Both pitting and filiform corrosion can access to the Mg alloy containing binary phase [16–18]. The general and pitting corrosion behavior of parent and FSW nugget regions were nearly the same, even though they were different in the untreated condition. The corrosion morphology of the AM50 alloy was predominantly controlled by the β phase distribution. Pitting corrosion was discerned in the welds [19,20].

Table 1a
Chemical composition (wt%) of AZ61A Mg alloy.

Al	Zn	Mn	Mg
5.45	1.26	0.17	Balance

Table 1b
Mechanical properties of AZ61A Mg alloy.

Yield strength (MPa)	Ultimate tensile strength (MPa)	Elongation (%)	Vickers hardness at 0.05 kg load (Hv)
177	272	8.40	57

From the literature review, it is understood that the most of the published information on corrosion behavior of Mg alloys were focused on pitting corrosion and stress corrosion of unwelded base alloys. Hence, the present investigation was carried out to study the effect of pH value, chloride ion concentration (Cl^-) and immersion time on corrosion rate of friction stir welded AZ61A magnesium alloy welds under immersion conditions.

2. Experimental procedure

2.1. Fabricating the joints and preparing the specimens

The material used in this study was AZ61A magnesium alloy in the form of extruded plates of 6 mm thickness. The chemical composition and mechanical properties of the base metal are presented in Tables 1a and 1b. The optical micrograph of base metal is shown in Fig. 1. The plate was cut to a required size (300 mm × 150 mm) by power hacksaw followed by milling. The square butt joint configuration was prepared to fabricate the joints. The initial joint configuration was obtained by securing the plates in position using mechanical clamps. The direction of welding was normal to the extruded direction. Single pass welding procedure was followed to fabricate the joints. A non-consumable tool made of high carbon steel was used to fabricate joints. An indigenously designed and developed computer numerical controlled FSW machine (22 kW; 4000 rpm; 60 kN) was used to fabricate joints. The FSW parameters were optimized by conducting trial runs and the welding conditions which produced defect free joints were taken as optimized welding conditions. The optimized welding conditions used to fabricate the joints in this investigation are presented in Table 2.

From the welded joints, the corrosion test specimens were extracted from the friction stir welds to the dimensions of 50 mm × 16 mm × 6 mm shown in Fig. 2. The specimens were ground with 500#, 800#, 1200#, 1500# grit SiC paper. Finally, it was cleaned with acetone and washed in distilled water then dried by warm flowing air. The optical micrograph of the friction stir weld region is shown in Fig. 3.

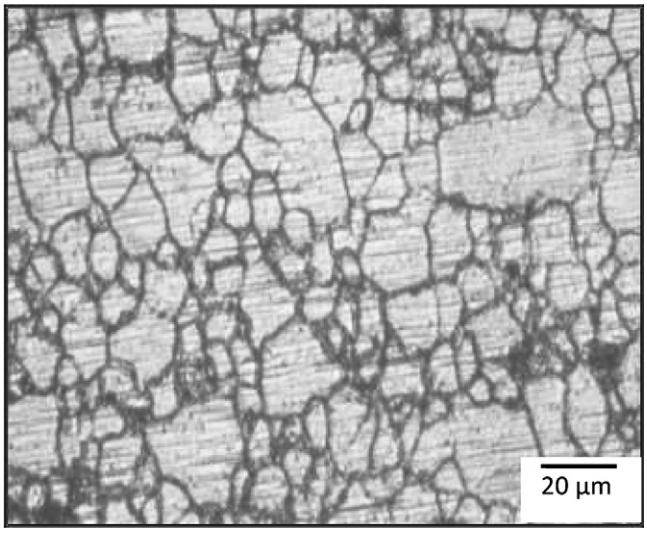

Fig. 1. Optical micrograph of AZ61A base metal.

Table 2
Optimized welding conditions and process parameters used to fabricate the joints.

Rotational speed (rpm)	Welding speed (mm/min)	Axial force (kN)	Tool shoulder diameter (mm)	Pin diameter (mm)	Pin length (mm)	Pin profile
1000	75	3	18	6	5	Left hand thread of 1 mm pitch

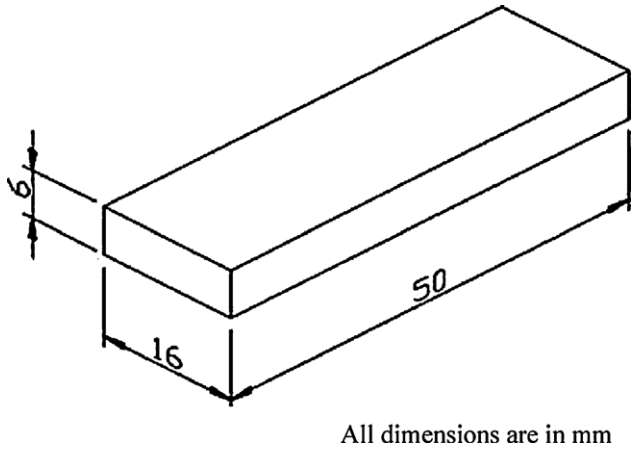

Fig. 2. Dimensions of corrosion test specimen.

2.2. Finding the limits of corrosion test parameters

From the literature [15,16], the predominant factors that have a greater influence on corrosion behavior of AZ61A magnesium alloy are identified. They are: (i) pH value of the solution, (ii) immersion time, (iii) chloride ion concentration. Large numbers of trial experiments were conducted to identify the feasible testing conditions using friction stir welded AZ61A magnesium alloy weld metal region under immersion conditions. The following inferences are obtained:

1. If pH value of the solution was less than 3, then the change in chloride ion concentration did not considerably affect the corrosion.
2. If the pH value was from 3 to 11, an inhibition of the corrosion process would occur stabilizing the protective layer.
3. If pH value was greater than 11, blocking of further corrosion by the active centers of protective layer took place.
4. If the chloride ion concentration was less than 0.2 M, visible corrosion did not occur in the experimental period.
5. If the chloride ion concentration was from 0.2 M to 1 M there was a reasonable fluctuation in the corrosion rate.
6. If the chloride ion concentration was greater than 1 M, rise in corrosion rate was slightly decreased.
7. If the immersion time was less than 1 h, the surface was completely covered with the thick and rough corrosion products and had an unpredicted corrosion rate.
8. If the immersion time was from 1 to 9 h, the tracks of the corrosion could be predicted.
9. If the immersion time was greater than 9 h, the tracks of corrosion film were difficult to identify.

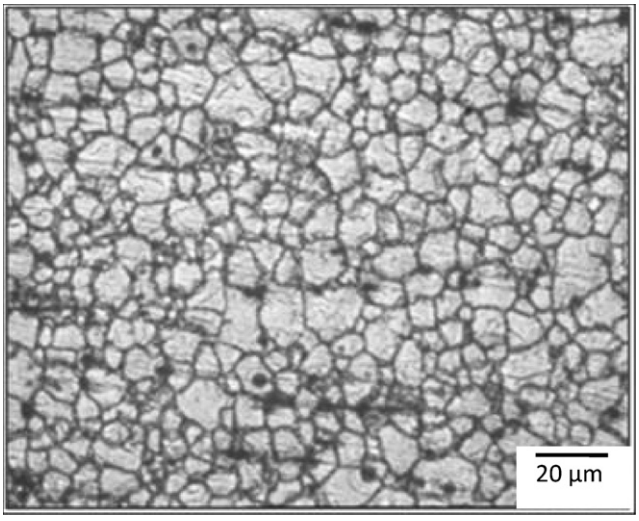

Fig. 3. Optical micrograph of stir zone of FSW AZ61A Mg alloy.

2.3. Developing the experimental design matrix

Owing to a wide range of factors, the use of three factors and central composite rotatable design matrix was chosen to minimize number of experiments. Design matrix consisting 20 sets of coded conditions (composing a full replication three factorial of 8 points, 6 corner points and 6 centre points) was chosen in this investigation. Table 3 presents the ranges of factors considered, and Table 4 shows the 20 sets of coded and actual values used to conduct the experiments.

For the convenience of recording and processing experimental data, the upper and lower levels of the factors were coded here as +1.682 and −1.682 respectively. The coded values of any intermediate value could be calculated using following relationship

$$X_i = \frac{1.682[2X - (X_{max} - X_{min})]}{X_{max} - X_{min}} \quad (1)$$

where X_i is the required coded value of a variable X and X is any value of the variable from X_{min} to X_{max}; X_{min} is the lower level of the variable; and X_{max} is the upper level of the variable.

2.4. Recording the responses (corrosion rate evaluation)

As per the ASTM standard (ASTM G1), the corrosion products were removed by immersing the specimens for one minute in a solution prepared by using 50 g chromium trioxide (CrO_3), 2.5 g silver nitrate ($AgNO_3$) and 5 g barium nitrate($Ba(NO_3)_2$) for 250 ml distilled water. These specimens were washed with distilled water, dried and weighed again to obtain the final weight (w_1). The weight loss (w) could be measured using the following relation,

$$w = w_o - w_1 \quad (2)$$

where w is the weight loss in g; w_o is the original weight before test in g; and w_1 is the final weight after test in g.

The corrosion rate of AZ61A FSW weld metal region could be calculated by using the following equation by conducting the immersion test as per the ASTM standard (ASTM G31)

$$\text{corrosion rate (mm/year)} = \frac{8.76 \times 10^4 \times w}{A \times D \times T} \quad (3)$$

where w is the weight loss in g; A is the surface area of the specimen in cm^2; D is the density of the material, 1.72 g/cm^3; and T is the corrosion time in h.

2.5. Metallography

Microstructural analysis was carried on the corroded specimens using a light optical microscope (Make: Union Optics, Japan; Model: VERSAMET-3) incorporated with an image analyzing software (Clemex-vision). The exposed specimen surface was prepared for the micro examination in the "as polished" conditions. The corrosion test specimens were polished in disc polishing machine with minor polishing and the surface was observed at 200× magnification. The corrosion products were analyzed by SEM-EDAX and XRD analysis.

3. Developing an empirical relationship

In the present investigation, to correlate the immersion test parameters and the corrosion rate of welds, a second order quadratic model was developed. The response (corrosion rate) is a function of pH value (P), immersion time (T) and chloride ion concentration (C) and it can be expressed as,

$$\text{corrosion rate (CR)} = f(P, T, C) \quad (4)$$

Table 3
Important factors and their levels.

S. No.	Factor	Unit	Notation	Levels				
				−1.682	−1	0	+1	+1.682
1	pH value		P	3	4.62	7	9.38	11
2	Immersion time	Hours (h)	T	1	2.62	5	7.38	9
3	Cl^- concentration	Mole (M)	C	0.2	0.36	0.6	0.84	1

The empirical relationship must include the main and interaction effects of all factors and hence the selected polynomial is expressed as follow:

$$Y = b_0 + \sum b_i x_i + \sum b_{ii} x_i^2 + \sum b_{ij} x_i x_j \quad (5)$$

For three factors, the selected polynomial can be expressed as

$$\text{corrosion rate (CR)} = b_0 + b_1(P) + b_2(T) + b_3(C) + b_{11}(P^2) + b_{22}(T^2) + b_{33}(C^2) + b_{12}(PT) + b_{13}(PC) + b_{23}(TC) \quad (6)$$

where b_0 is the average of responses (corrosion rate) and $b_1, b_2, b_3, \ldots, b_{11}, b_{12}, b_{13}, \ldots, b_{22}, b_{23}, b_{33}$, are the coefficient that depend on the respective main and interaction factors, which are calculated using the expression given below,

$$B_i = \sum \frac{X_i, Y_i}{n} \quad (7)$$

where '*i*' varies from 1 to *n*, in which X_i is the corresponding coded value of a factor and Y_i is the corresponding response output value (corrosion rate) obtained from the experiment and '*n*' is the total number of combination considered. All the coefficients were obtained applying central composite rotatable design matrix using the Design Expert statistical software package. After determining the significant coefficients (at 95% confidence level), the final relationship was developed including only these coefficients. The final empirical relationship obtained by the above procedure to estimate corrosion rate of friction stir welds of AZ61A magnesium alloy is given below:

$$\text{corrosion rate (CR)} = 4.81 - 0.83(P) - 0.41(T) + 1.09(C) + 0.41(PT) - 0.43(PC) + 0.28(P^2) + 1.019(C^2) \ \text{(mm/year)} \quad (8)$$

The analysis of variance (ANOVA) technique was used to find the significant main and interaction factors. The results of second order response surface model fitting as analysis of variance (ANOVA) are given in Table 5. The determination coefficient (r^2) indicates the goodness of fit for the model. The Model *F*-value of 31.30 infers the model is significant. There was only a 0.01% chance that a "Model F-Value" this large could occur due to noise. Values of "Prob > *F*" less than 0.0500 indicated model terms were significant. In this case *P*, *T*, *C*, *PT*, *PC*, P^2 and C^2 are significant model terms. Values greater than 0.1000 indicate the model terms are not significant.If there are many insignificant model terms (not counting those required to support hierarchy), model reduction may improve your model. The "Lack of Fit *F*-value" of 3.03 implies the Lack of Fit is not significant relative to the pure error. There is a 12.47% chance that a "Lack of Fit *F*-value" this large could occur due to noise. Non-significant lack of fit is good – we want the model to fit. All this indicated an excellent suitability of the regression model. Each of the observed values compared with the experimental values shown in Fig. 4

3.1. Validation of the developed models

To validate the developed models, three confirmation experiments were carried out with the process parameters chosen randomly close the range of experimental parameters. For the actual responses the average of three measured was calculated. Table 6 summarizes the experimental condition, the average actual experimental values, the predicted values and the percentage error. The optimum values of process parameters and the corrosion rate of friction stir welded AZ61A magnesium alloy welds shows the excellent agreement with the predicted values.

Table 4
Design matrix and experimental results.

Ex. No.	Coded values			Actual values			Weight loss (g)	Corrosion rate (mm/year)[a]
	pH	Time (h)	Conc. (M)	pH	Time (h)	Conc. (M)		
1	−1	−1	−1	4.62	2.62	0.36	0.776	6.32 (0.12)
2	+1	−1	−1	9.38	2.62	0.36	0.568	4.62 (0.58)
3	−1	+1	−1	4.62	7.38	0.36	1.604	4.63 (0.74)
4	+1	+1	−1	9.38	7.38	0.36	1.383	3.99 (0.21)
5	−1	−1	+1	4.62	2.62	0.84	2.860	9.60 (0.2)
6	+1	−1	+1	9.38	2.62	0.84	0.691	5.62 (0.08)
7	−1	+1	+1	4.62	7.38	0.84	2.922	8.43 (0.04)
8	+1	+1	+1	9.38	7.38	0.84	2.305	6.65 (0.05)
9	−1.682	0	0	3	5	0.60	1.550	6.60 (0.21)
10	+1.682	0	0	11	5	0.60	1.091	4.65 (0.27)
11	0	−1.682	0	7	1	0.60	1.458	6.21 (0.21)
12	0	+1.682	0	7	9	0.60	0.205	4.36 (0.38)
13	0	0	−1.682	7	5	0.20	2.726	6.45 (0.51)
14	0	0	+1.682	7	5	1	2.101	8.95 (0.13)
15	0	0	0	7	5	0.60	1.070	4.56 (0.16)
16	0	0	0	7	5	0.60	1.310	5.54 (0.12)
17	0	0	0	7	5	0.60	1.073	4.57 (0.28)
18	0	0	0	7	5	0.60	1.082	4.61 (0.26)
19	0	0	0	7	5	0.60	1.094	4.66 (0.01)
20	0	0	0	7	5	0.60	1.139	4.85 (0.10)

[a] The values presented in parentheses are standard deviation.

Table 5
ANOVA test results.

Source	Sum of squares	df	Mean square	*F*-Value	*p*-Value Prob > *F*	
Model	26.16	9	2.91	29.22	<0.0001	Significant
P	2.76	1	2.76	27.7	0.0004	
T	19.41	1	19.41	195.19	<0.0001	
C	1.08	1	1.08	10.88	0.0080	
PT	0.65	1	0.65	6.54	0.0285	
PC	0.097	1	0.097	0.98	0.3461	
TC	0.49	1	0.49	4.93	0.0507	
P2	0.24	1	0.24	2.39	0.1534	
T2	1.22	1	1.22	12.23	0.0057	
C2	0.056	1	0.056	0.57	0.4686	
Residual	0.099	10	0.099			
Lack of fit	0.62	5	0.12	1.63	0.3036	Not significant
Pure error	0.38	5	0.076			
Cor total	27.15	19				

Table 6
Validation test results.

Experimental details					Results
Input parameters					Responses
Ex. No.	pH	Exposure time (h)	Chloride ion conc. (M)		Corrosion rate (mm/year)
21	4	2	0.4	Actual	7.35
				Predicted	7.61
				Error %	3.2%
22	8	6	0.8	Actual	6.75
				Predicted	6.94
				Error %	2.7%
23	6	4	0.6	Actual	4.1
				Predicted	4.23
				Error %	3.0%

4. Results and discussion

From Table 4, it shows the corrosion rate obtained from immersion tests at different pH value, chloride ion concentration and immersion time. Fig. 5 shows the normalized weight loss of immersion test samples underwent corrosion and the normalized corrosion rate of immersion test samples was shown in the bar chart (Fig. 6). The highest corrosion rate was observed at pH 3 and at neutral pH, the corrosion rate was remained constant about and comparatively low corrosion rate was observed in alkaline solution. It was seen that the influence of pH was more at higher concentration as compared to lower concentration in neutral and alkaline solutions [16]. At all pH values, the FS weld metal exhibited a rise in corrosion rate with the decrease in pH value. In the neutral pH, the corrosion rate remained constant approximately

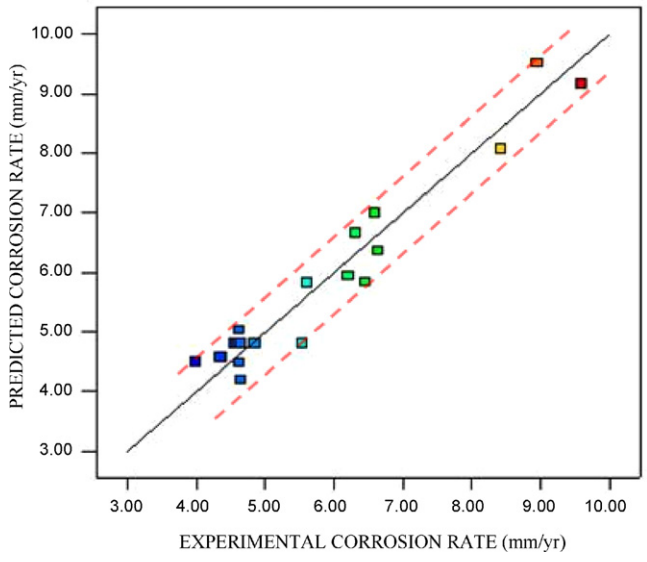

Fig. 4. Correlation graph for response (corrosion rate).

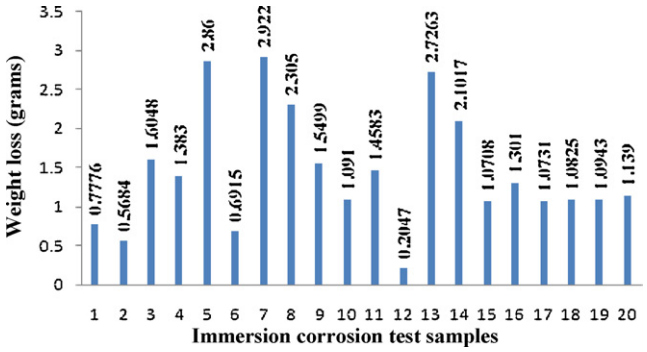

Fig. 5. Normalized weight loss of immersion corrosion test samples.

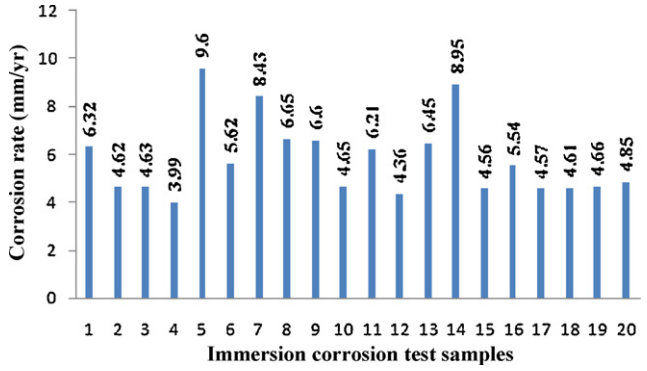

Fig. 6. Normalized corrosion rate of immersion corrosion test samples.

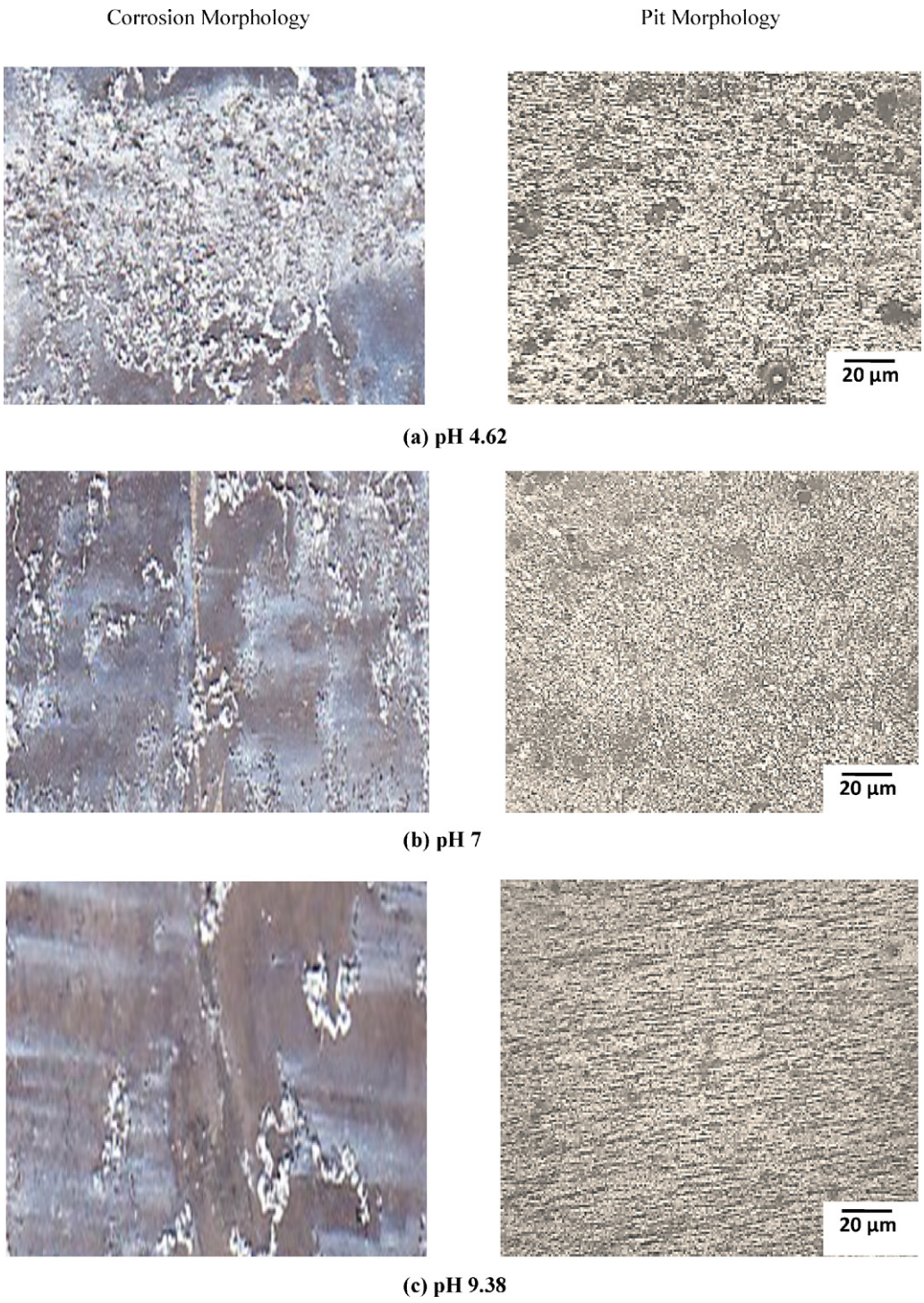

Fig. 7. Effect of pH on corrosion morphology and pit morphology.

and a comparatively low corrosion rate was observed in alkaline solutions. It was also observed that corrosion rates of friction stir welded AZ61A Mg alloy was quite comparable with the corrosion rates of referred articles of same series of magnesium alloys.

4.1. Corrosion mechanism

The effect of pH of the solutions on the corrosion behavior is in agreement with *E*–pH diagram of magnesium and aluminum. The following points illustrate the mechanisms for all types of corrosion of magnesium alloys.

In acidic media: Highly acidic solutions are aggressive for both the magnesium and aluminum. In acidic media, probably, anodic dissolution was held. Hydrogen evolution is intimately associated with magnesium dissolution in two separate ways; an electrochemical reaction governed by Eq. (9) balances the magnesium dissolution reaction, Eq. (10)

$$2H^+ + 2e^- \rightarrow H_2 \text{ (cathodic partial reaction)} \quad (9)$$

$$2Mg \rightarrow 2Mg^+ + 2e^- \text{ (anodic partial reaction)} \quad (10)$$

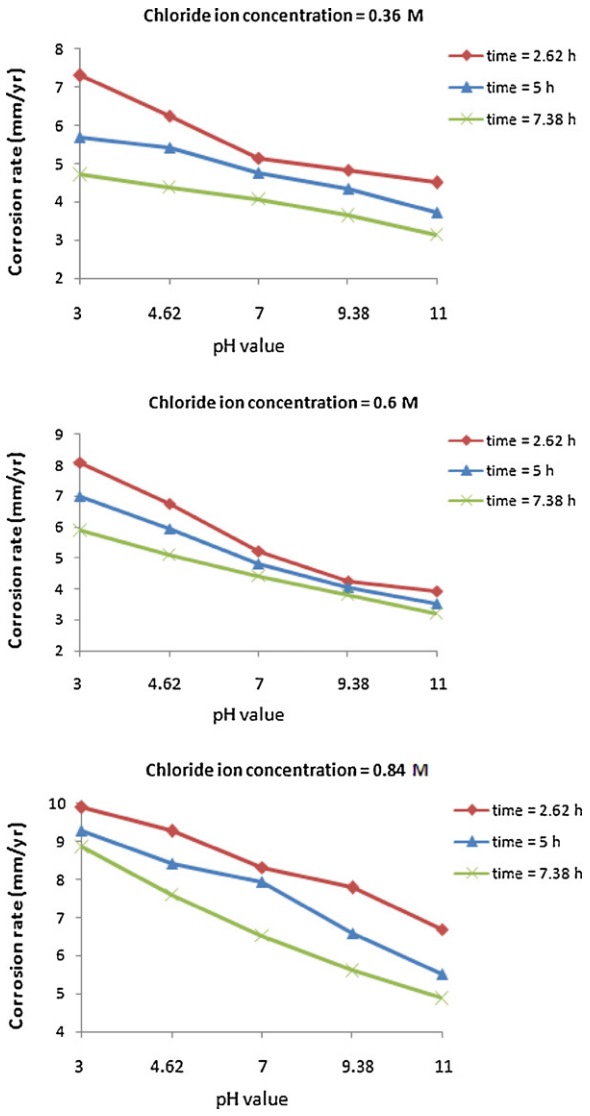

Fig. 8. Effect of pH value on corrosion rate.

In neutral media: The corrosion rate was decreases with the increase of pH towards neutral region. This may be due to the less aggressiveness of the solution and also as this pH fails in the passive region for aluminum if not for magnesium. In addition, hydrogen is also produced directly in the reaction of Mg^{+} with water by Eq. (11). The overall reaction, Eq. (12), produces one molecule of hydrogen gas for each atom of magnesium dissolved. Furthermore, the overall reaction consumes H^{+} and produces OH^{-}, i.e., the pH increases, which favor the formation of a magnesium hydroxide film by the precipitation reaction.

$$2Mg^{+} + 2H_2O \rightarrow 2Mg^{2+} + 2OH^{-} + H_2\,(\text{chemical reaction}) \quad (11)$$

$$2Mg + 2H^{+} + 2H_2O \rightarrow 2Mg^{2+} + 2OH^{-} + 2H_2\,(\text{overall reaction}) \quad (12)$$

In alkaline media: In agreement with the above equations, if the pH was above 9, favors the formation of the protective hydroxide film, Eq. (13) (depending upon the concentration of magnesium in solution). The most probable reason is that the cathodic reaction is the liberation of hydrogen as given by Eq. (14). A byproduct of that cathodic reaction is the production of OH^{-} (or equivalently the consumption of H^{+}) with a concomitant increase of the pH and the stabilization of the local magnesium hydroxide film and decrease in corrosion tendency. Thus localized corrosion in magnesium has an inherent tendency to be self-limiting.

$$Mg^{2+} + 2OH^{-} \rightarrow Mg(OH)_2\,(\text{product formation}) \quad (13)$$

The chance development of areas of localized corrosion leads to the undermining and falling out of particles of magnesium, even in the corrosion of pure magnesium. In the present study, the formation of $Mg(OH)_2$ in corrosion media with starting pH 3 does not mean that these products are stable at this pH value. Since the corrosion attack was localized in magnesium alloys, a model of pitting corrosion mechanism was shown below, Firstly, the alloy has a protective oxide film in air. When it is immersed in a sodium chloride aqueous solution, Cl^{-} ions will absorb on α areas bordering on $Mg_{17}Al_{12}$ particles. If the breakdown potential of the oxide film reaches its free corrosion potential ($E_{corr} \sim -1.53$ V for AZ series magnesium alloys), then the α-matrix as an anode, compared to $Mg_{17}Al_{12}$ particles, starts to dissolve, and a corrosion nucleus may form nearby an $Mg_{17}Al_{12}$ particle. The nucleus develops a corrosion pit, this may result in $Mg(OH)_2$ formation and hydrogen evolution according to the chemical reactions

Anodic reaction:

$$Mg \rightarrow Mg^{2+} + 2e^{-} \quad (14)$$

Cathodic reaction:

$$2H_2O + 2e \rightarrow 2OH^{-} + H_2\uparrow \quad (15)$$

Total reaction:

$$Mg^{2+} + 2H_2O \rightarrow Mg(OH)_2 + 2H_2\uparrow \quad (16)$$

4.2. Influence of pH value on corrosion rate

Fig. 7 shows the effect of pH on corrosion morphology and pit morphology of the corrosion test specimen immersed in 0.6 M concentration of NaCl for 5 h with different pH values of pH 4.62, pH 7 and pH 9.38. It was seen that, at lower concentration, the surface of the specimen was relatively slightly corroded in neutral and alkaline solutions while severely corroded at all pH values at higher chloride ion concentrations. The corrosion of FSW weld metal region was significantly influenced by pH.

The dissolution of magnesium in aqueous solutions proceeded by the reduction of water to produce magnesium hydroxide $Mg(OH)_2$ and hydrogen gas (H_2). The reduction process was primarily water reduction. These reactions are reported to be insensitive to oxygen concentration.

$$Mg \rightarrow Mg^{2+} + 2e^{-} \quad (17)$$

$$2H_2O + 2e^{-} \rightarrow 2OH^{-} + H_2 \quad (18)$$

$$Mg^{2+} + 2OH^{-} \rightarrow Mg(OH)_2 \quad (19)$$

Highly acidic solutions are aggressive towards magnesium, hence a very high corrosion rate. In magnesium–aluminum alloys, a pH above 9 favors the formation of $Mg(OH)_2$ (depending on the concentration of the medium). This corrosion behavior is consistent with the current understanding that the corrosion behavior of magnesium alloys was governed by the characteristics of its surface film [16]. The surface film on magnesium alloys in aqueous solutions is thought to be mainly $Mg(OH)_2$. Eq. (11) describes the surface film formation, this occurs because Mg^{2+} has a low solubility. The influence of pH needs to be taken into account the magnesium *E*–pH diagram (Pourbaix diagram). However, even though the surface film is not thermodynamically stable at low pH values, the dissolution kinetics may be slow and surface film may be formed provided the dissolution kinetics are slower than the formation kinetics [17].

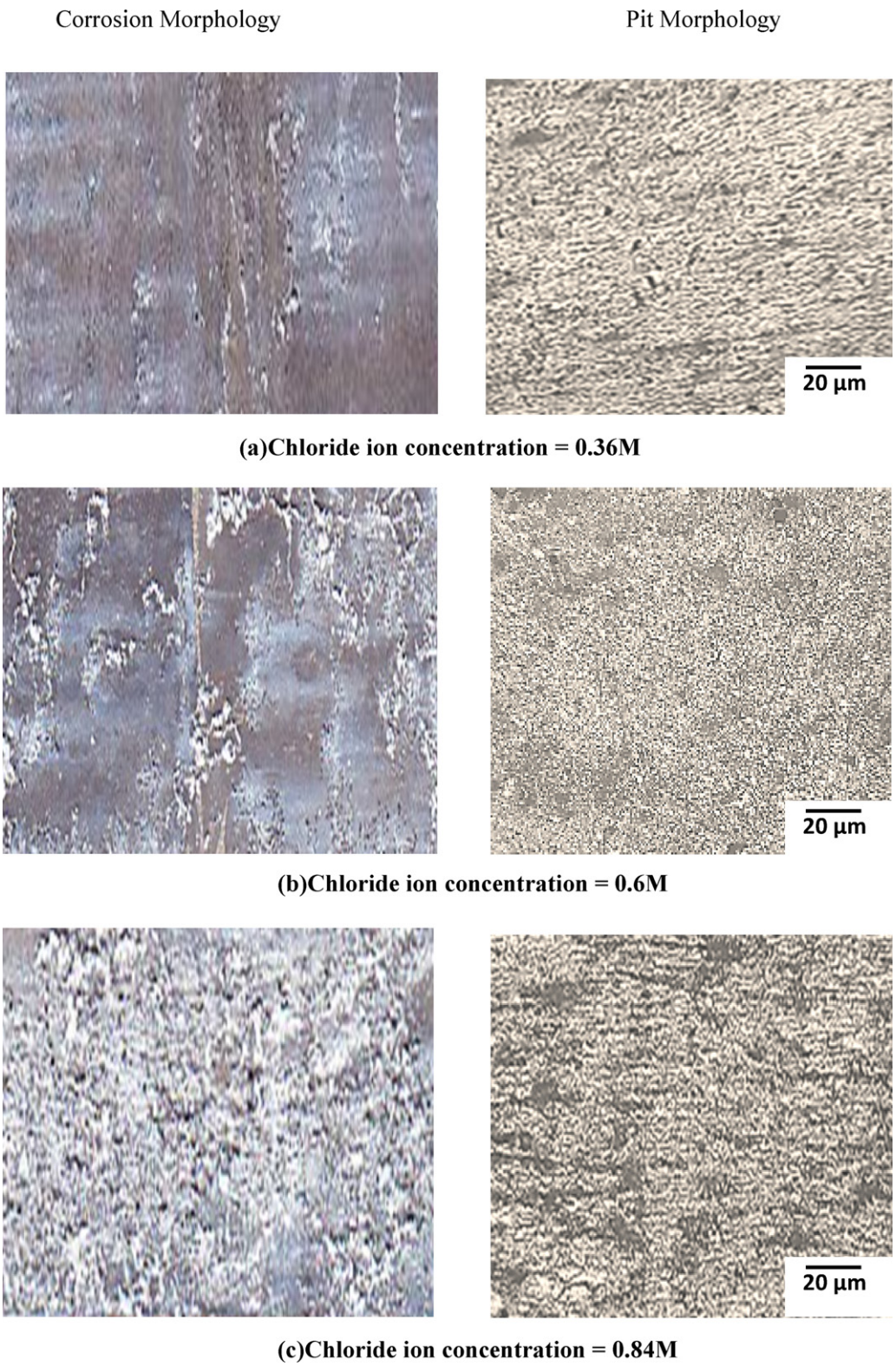

Fig. 9. Effect of chloride ion concentration on corrosion morphology and pit morphology.

From the pit morphology of FS weld metal after immersion test, it was observed that the matrix shows the pitting marks and the pitting corrosion that has taken places at the friction stir welded microstructure. The particles were Mn–Al compound and fragmented $Mg_{17}Al_{12}$. After welding, the β-phases are precipitated as $Mg_{17}Al_{12}$. The β-phase is rearranged in welding direction. It was found that the β-phases are spread adjacent to the grain boundaries and seems discontinuous. As a result, the distribution is characterized by a stringer-shaped. The number of pits was more in the weld metal region when it was immersed in the solution of low

pH. Hence, the corrosion rate increases with the decrease in pH value. Since the increase of grain and grain boundary in the weld metal region, the grains boundary acts cathodic to grains causing micro galvanic effect. Corrosion tends to be concentrated in the area's adjacent to the grain boundary until eventually the grain may be undercut and fall out. The β-phase plays an important role in the corrosion resistance of Magnesium alloys. It was noted that the β-phase might serve as a galvanic cathode and accelerate the corrosion of the α-matrix if the distribution of the β-phase is discontinuous. For the anodic process, due to the stringer-shaped distribution of the β-phase, the β-phase will be less effective barrier against anodic dissolution. Accordingly, the anodic dissolution process is accelerated after welding, and the corrosion zones spread along the β-phase stringer.

Fig. 8 shows the graph representing the effect of pH value on corrosion rate. The graph shows clearly that the corrosion rate was decreased with the increase in pH value. At every chloride ion concentration and immersion time, the weld metal usually exhibited a decrease in corrosion rate with increase in pH. In neutral pH, the corrosion rate was remained constant approximately and comparatively low corrosion rate was observed in alkaline solution. It was seen that the influence of pH was more at higher concentration as compared to lower concentration in neutral and alkaline solutions.

4.3. Influence of chloride ion concentration on corrosion rate

Fig. 9 shows the effect of chloride ion concentration on corrosion morphology and pit morphology of the anodic specimen immersed in NaCl solution of pH 5 for exposure time 5 h with different chloride ion concentration of 0.36 M, 0.6 M and 0.84 M solutions. It was observed that, the surface of the weldments was covered with corrosion products increase in ratio, with the increase of chloride ion concentration. The corrosion rate of the weldments also increased with increasing chloride ion concentrations. The increase in corrosion rate with the increasing chloride ion concentration was attributed to the participation of chloride ions in the dissolution reaction. Chloride ions are very aggressive to magnesium. The adsorption of chloride ions to oxide covered magnesium surface transforms $Mg(OH)_2$ to easily soluble $MgCl_2$ [18]. It was considered that the corrosion becomes severe owing to the penetration of hydroxide film by Cl^- ion and thereby the formation metal hydroxyl chloride complex which governed the following reaction,

$$Mg^{2+} + 2H_2O + 2Cl^- \rightarrow 2Mg(OH)_2Cl_2 \quad (20)$$

This corrosion behavior was consistent with the current understanding that the corrosion behavior of magnesium alloys was governed by a partially protective surface film with the corrosion reaction occurring predominantly at the breaks or imperfections of the partially protective film. The implication is that the fraction of film free surfaces increases with increasing chloride ion concentration. This is consistent with the known tendency of chloride ions to cause with the film breakdown [21].

From the pit morphology of FS weld metal, it was found that many dispersed pits were seen on the specimen and the morphology shows typical characteristics of localized corrosion. The FS weld metal exhibited a rise in corrosion rate with increase in Cl^- concentration and thus the change of Cl^- concentration affected the corrosion rate much more in higher concentration solutions than that in lower concentration solutions. When more Cl^- in NaCl solution promoted the corrosion, the corrosive intermediate (Cl^-) would be rapidly transferred through the outer layer and reached the substrate of the alloy surface. Hence, the corrosion rate was increased.

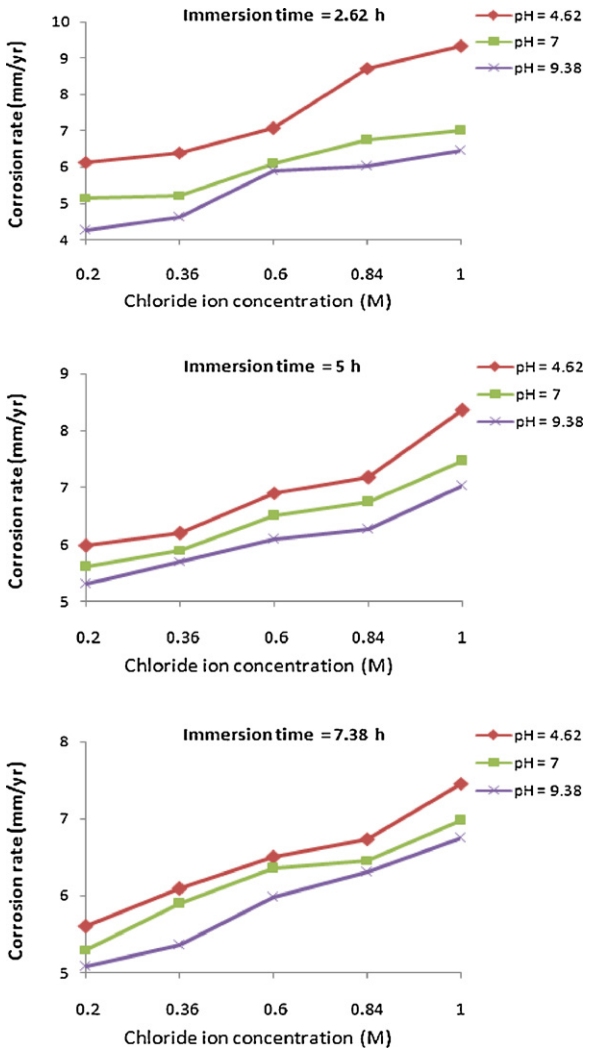

Fig. 10. Effect of chloride ion concentration on corrosion rate.

Fig. 10 shows the graph represents the effect of chloride ion concentration on corrosion rate. The graph shows clearly that the corrosion rate was increased with the increase in chloride ion concentration. From the morphological studies, it was observed that, at lower concentration, the surface of the specimen relatively slightly corroded; while severely corrode in the higher concentrations.

4.4. Influence of immersion time on corrosion rate

Fig. 11 shows the effect of spraying time on corrosion morphology and pit morphology of the weldments sprayed with NaCl solution of pH5 with chloride ion concentration 0.6 M with different spraying time of 2.62 h, 5 h and 7.38 h solutions. It proves that the initial corrosion product impeded the passage of corrosion medium and provided protection for the metal substrate. In long time immersion with magnesium dissolution and hydrogen evolution, the pH value of the solution will increase, namely basification. Basification should be propitious to the formation of passive film, which can protect the alloy [21,22]. The insoluble corrosion products on the surface of the alloy could slow down the corrosion rate.

Furthermore, the grain is refined and quite lots of β particles distribute continually along the grain boundary. In this case, β phase particles cannot be easily destroyed and, with the increase of corrosion time, the quantity of β phases in the exposed

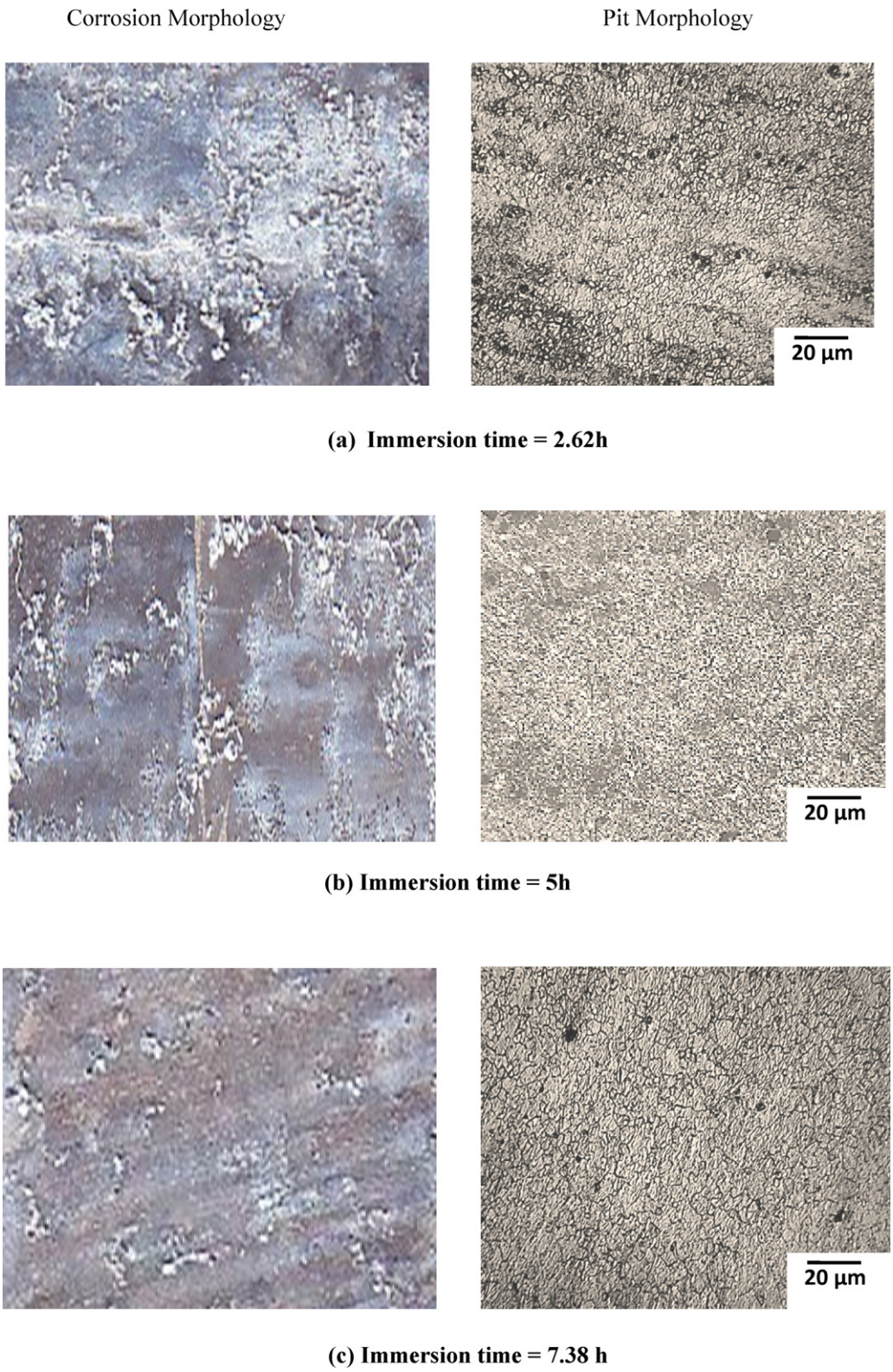

Fig. 11. Effect of immersion time on corrosion morphology and pit morphology.

surface would increase and finally play the role of a corrosion barrier [22]. Although there were some grains of α phase still being corroded, most of them remained α phase grains which were protected under the β phase barrier, so that the corrosion rate would be decreased with the increase in immersion time.

Fig. 12 shows the graph represents the effect of immersion time on corrosion rate. The graph shows clearly that the corrosion rate was decreased with the increase in immersion time. It results that there was an increase in hydrogen evolution with the increasing immersion time, which tends to increase the concentration of OH^- ions strengthening the surface from corrosion causing further.

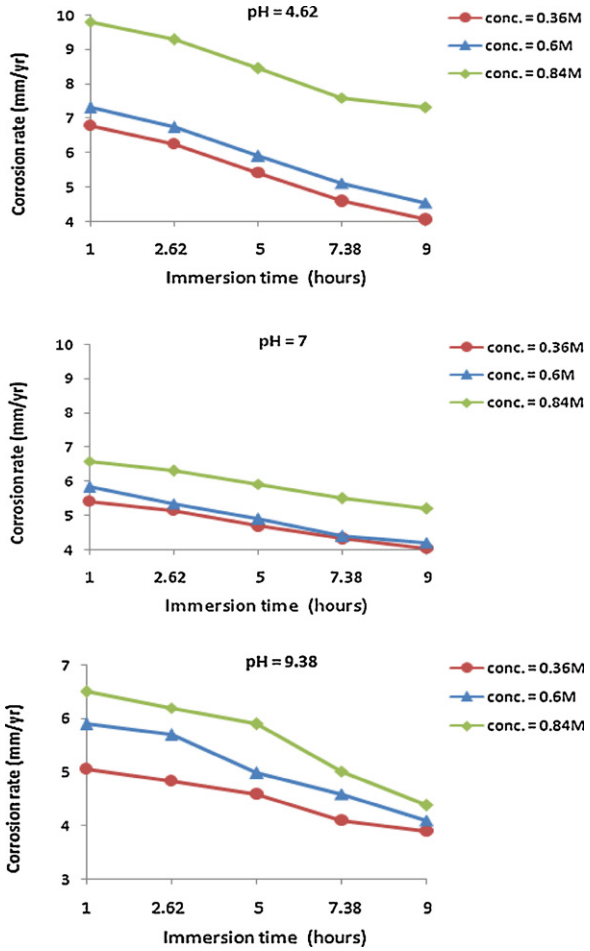

Fig. 12. Effect of immersion time on corrosion rate.

Thus the corrosion rate decreased with the increase in immersion time.

4.5. SEM and XRD analysis

Fig. 13 shows the SEM morphology of the corroded specimen underwent immersion tests with the experiment no. 1, 8 and 15. Fig. 11(a) shows the specimen composed of more localized attack. With pH as a factor, the decrease in pH tends to attack very localized on the surface, and later, it penetrates to the substrates, causing higher corrosion and its rate. The localized attack in the specimen formed at the grains. Since the increase in grain and grain boundary in the FSW welds, the grain boundary acts cathodic to grain, enhancing micro-galvanic effect. Corrosion tends to be concentrated in the area adjacent to the grain boundary until eventually the grain may be undercut and fall out [23].

Fig. 13(b) shows more cracks over the corrosion products, where the Cl^- penetrates into the surface. When more Cl^- in NaCl solution promoted the corrosion, the corrosive intermediate (Cl^-) would be rapidly transferred through the outer layer and reached the substrate of the alloy surface. Hence, the corrosion rate was increased [23].

Fig. 13(c) shows more corrosion products and the corrosion products comprises of the hydroxide layer. Since, with the increase in immersion time, the hydroxide layer formed is the dominant factor to avoid further corrosion. This is attributed to corrosion occurring over increasing fraction of the surface was observed, which is the insoluble corrosion products $Mg(OH)_2$. Thus, the corrosion rate decreases with the increase of immersion time.

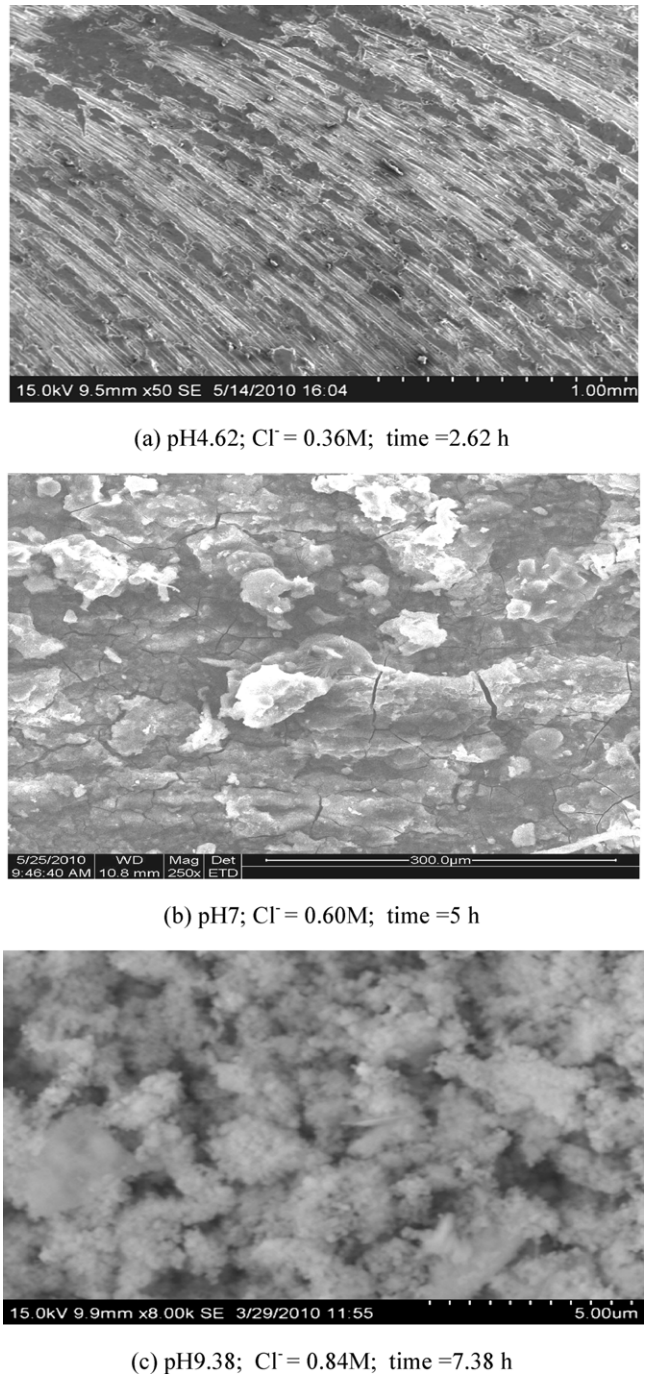

(a) pH4.62; Cl^- = 0.36M; time =2.62 h

(b) pH7; Cl^- = 0.60M; time =5 h

(c) pH9.38; Cl^- = 0.84M; time =7.38 h

Fig. 13. Scanning electron micrograph of immersion corrosion test specimens.

Fig. 14 shows the XRD analysis to predict the composition of corrosion products and phase in the specimen subjected to galvanic corrosion tests. All the characteristic peaks originate from the metallic Mg substrate and the β phase. However, $Mg(OH)_2$ phase is detected in the specimen. Besides, many small peaks are present in the patterns from 10° to 30°, which could not be attributed to a single compound. They are most likely associated with $Mg_5(CO_3)_4(OH)_2{\cdot}8H_2O$ considering that CO_2 naturally present. $Mg(OH)_2$ is dominant product in the corrosion zone. $Mg(OH)_2$ (brucite) has a hexagonal crystal structure and undergoes easily basal cleavage causing cracking and curling in the film [24]. Certain peaks of β-phase exist which enhances the corrosion resistivity with the increment of immersion time.

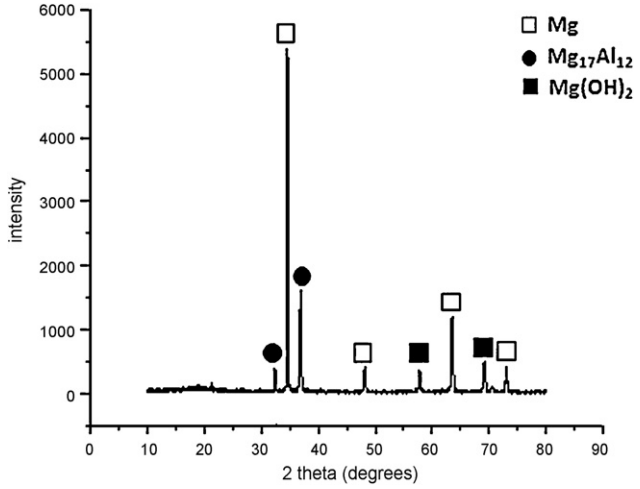

Fig. 14. XRD pattern of immersion corrosion test specimen.

5. Conclusions

The friction stirs welded AZ61A magnesium alloy welds exhibited an increment in the corrosion resistance with the increase in pH. The corrosion rate was higher at the acidic media than at the alkaline and neutral media with same concentrations and immersion time.

The friction stirs welded AZ61A magnesium alloy welds corroded more seriously with the increase in Cl^- concentrations. More the Cl^- promoted the corrosion along with the rise in corrosion rate.

The corrosion resistance was formed in the friction stirs welded AZ61A magnesium alloy welds with the increased immersion period. A corrosion resistivity prevails with the increase of immersion time, resulting with the formation of hydroxide layer as a dominant factor to avoid the corrosion further.

Acknowledgements

The authors would like to thank Centre for Materials Joining & Research (CEMAJOR), Department of Manufacturing Engineering, Annamalai University, Annamalai Nagar, for extending the facilities of Materials Joining Laboratory and Corrosion Testing laboratory to carry out this investigation.

References

[1] A. Pardo, M.C. Merino, A.E. Coy, R. Arrabal, F. Viejo, E. Matykina, Corros. Sci. 50 (2008) 823–834.
[2] ASTM G31-72, Standard practice for laboratory immersion corrosion testing of metals, vol. 03.02.2004, 2004.
[3] G. Song, A. Aterns, Adv. Eng. Mater. 5 (2003) 837–858.
[4] B.A. Shaw, in: L.J. Korb, ASM (Eds.), ASM Handbook, vol. 13A: Corrosion, 9th ed., ASM International Handbook Committee, Metals Park, 2003, p. 692.
[5] D.L. Hawke, J.E. Hillis, M. Pekguleryuz, I. Nkatusugawa, in: M.M. Avedesian, H. Baker (Eds.), Magnesium and Magnesium Alloys, ASM International, Materials Park, 1999, pp. 194–210.
[6] G. Song, A. Atrens, Adv. Eng. Mater. 9 (2007) 177.
[7] R. Tunold, H. Holton, M.-B.H. Berge, A. Lasson, R. Steen-Hansen, Corros. Sci. 17 (1977) 353.
[8] G. Song, A. Atrens, Adv. Eng. Mater. 5 (2003) 837.
[9] G. Song, A. Atrens, D. St John, J. Nairn, Y. Li, Corros. Sci. 39 (1997) 855.
[10] A. Atrens, R. Coade, J. Allison, H. Kohl, G. Hochoertler, G. Krist, Mater. Forum 17 (1993) 263.
[11] G. Song, A. Atrens, B. Wu, X. Zhang, Corros. Sci. 40 (1998) 1769–1791.
[12] R. Ambat, N. Aung, W. Zhao, Corros. Sci. 42 (2000) 1433–1455.
[13] M.C. Merino, A. Pardo, R. Arrabal, S. Merino, P. Casajus, M. Mohedano, Corros. Sci. 52 (2010) 1696–1704.
[14] N. Hara, Y. Kobayashi, D. Kagaya, N. Akao, Corros. Sci. 49 (2007) 166–175.
[15] P. Schumtz, V. Guiaumin, R.S. Lilard, J.A. Lilard, G.S Frankela, J. Electrochem. Soc. 150 (2003) B99–B110.
[16] W.C Neil, M. Forsyth, P.C. Howlettt, C.R. Hutchison, B.R.W Hinton, Corros. Sci. 51 (2009) 387–394.
[17] A.M. Lafront, W. Zhang, S. Jin, R. Tremblay, D. Dube, E. Ghali, Electrochim. Acta 51 (2005) 489–501.
[18] R.-C. Zeng, J. Chen, W. Dietzel, R. Zettler, J.F. dos Santos, M.L. Nascimento, K.U. Kainer, Corros. Sci. 51 (2009) 1738–1746.
[19] H. Altun, S. Sen, Mater. Des. 25 (2004) 637–643.
[20] Y. Song, D. Shan, R. Chen, E.-H. Han, Corros. Sci. 52 (2010) 1830–1837.
[21] G. Song, A. Atrens, Adv. Eng. Mater. 5 (2003) 837–858.
[22] L. Wang, B.-P. Zhang, T. Shinohara, Mater. Des. 31 (2010) 857–863.
[23] L. Gao, C. Zhang, M. Zhang, X. Huang, N. Sheng, J. Alloys Compd. (2007) 285–289.
[24] H.P. Godard, W.B. Lepson, M.R. Bothewell, R.L. Kane, The Corrosion of Light Metals, Wiley, New York, 1967.